Check for updates

Insights into critical metal element migration and enrichment in coal gasification

Juan Cai,[a] Boyan Zhang,[a] Jiatao Dang,[b] Yunpeng Zhao, [ID][c] Dingcheng Liang, [ID][a] Qiang Xie,[a] Maohong Fan [ID][d] and Jinchang Liu [ID] *[a]

With the rapid development of China's semiconductor, military, and new energy industries, ensuring a stable supply and acquisition of critical metal elements, including lithium, gallium, germanium, and indium, has gained increasing attention. The migration and enrichment of critical metals during coal gasification can provide essential insights for developing metal extraction strategies from gasification slag. This work focused on the patterns of migration and enrichment of critical metal elements under varying gasification temperatures through comprehensive element distribution analysis and molecular structure characterization. Results show that the main component of gasification slag is mullite, which is composed of aluminate- and silicate-containing groups, namely, Si–O, O–Si–O, Al–O, and O–Al–O. As the gasification temperature increases from 1000 °C to 1500 °C, lithium, gallium, and germanium exist in the residual state, while the enrichment state of indium is complex. The concentrations of the residual state of each element gasified at 1500 °C are 121.2 µg g^{-1}, 46.93 µg g^{-1}, 0.12 µg g^{-1}, and 0.03 µg g^{-1}. However, lithium is mainly associated with clay minerals in coal slag. Meanwhile, gallium exhibits a relatively high bonding affinity for aluminates and silicates in the slag when the gasification temperature exceeds 1400 °C. By contrast, germanium and indium are demonstrated to have low affinity for aluminates and silicates in coal gasification slag. Germanium has more potential to combine with sulfur than aluminates and silicates, as revealed through enrichment factor analysis. Indium displays a complicated occurrence form in coal slag, demonstrating a better bonding affinity for oxygen and hydrogen in high-temperature gasification.

1. Introduction

Coal gasification refers to the process in which pulverized coal reacts with an oxidizing agent under high-temperature and high-pressure conditions within a gasifier.[1,2] During this process, organic compounds are completely oxidized to produce syngas, while inorganic minerals remain in the coal melt and combine to form coarse and fine gasification slag.[3,4] Coarse slag accounts for around 70% of the total slag produced, while fine slag makes up about 30%.[5–8] China, a major coal consumer, has accumulated hundreds of millions of tons of gasification slag, with an annual emission rate rapidly increasing to 35 million tons owing to the lack of large-scale reduction and disposal technologies. The current utilization efficiency of gasification slag is <50%, emphasizing the need for developing high-value-added approaches for its utilization.[9–11] Clean coal processing and utilization technology is essential for the sustainable development of the economy and crucial for ecological environmental protection. Coal gasification, as an efficient and clean coal utilization technology, lies at the core of modern coal chemical technology.[12] Coal-associated metals serve as a valuable supplement to traditional metal deposits.[13,14]

Lithium, gallium, germanium, and indium are considered critical metals in China's frontier science breakthroughs.[15–18] Lithium is known as the "green energy metal" and has wide applications in energy storage, chemical industries, medicine, metallurgy, and electronics industries.[19,20] The main lithium minerals in nature include spodumene, lepidolite, petalite, and lucinite. Liquid ores containing lithium mainly consist of salt lake brine, underground brine, and hot springs. The lithium resources in coal in China are primarily distributed in the Carboniferous–Permian strata in northern China, among which the most important carriers of lithium are chlorite.[13,21,22] Gallium has been explored for its potential applications in various fields, including the electronics industry, heat dissipation, flexible devices, and biomedicine. Gallium is a scarce metallic element with a strong affinity for inorganic constituents primarily present in coal, such as kaolinite, diaspore, and

*a*School of Chemical & Environmental Engineering, China University of Mining and Technology (Beijing), Beijing 100083, China. E-mail: liujinchang@cumtb.edu.cn

*b*College of Mechanical & Electrical Engineering, Henan Agricultural University, Zhengzhou 450002, Henan, China

*c*Key Laboratory of Coal Processing and Efficient Utilization, Ministry of Education, China University of Mining and Technology, Xuzhou 221116, Jiangsu, China

*d*College of Engineering and Physical Sciences, School of Energy Resources, University of Wyoming, Laramie, WY, 82071, USA

boehmite.[23,24] Previous research has demonstrated the analogous chemical properties between gallium and aluminum, enabling gallium to substitute aluminum within the mineral lattice through an isomorphic mechanism. Thus, kaolinite predominantly serves as the carrier of gallium in coal.[13,25] Germanium is an excellent semiconductor that can be used for producing precision devices, catalysts, and fluorescent materials. Germanium occurs naturally in diverse states in coal by combining with organic components to form germanium-containing organic compounds or chelates. In addition, germanium can occur in clay minerals in an inorganic state, and a tiny amount of germanium exists in a water-soluble and ion-exchangeable state in coal. Indium is primarily utilized to produce low-melting alloys, semiconductors, and electric devices. The presence of indium in coal mainly originates from its inorganic components, existing as both organic and inorganic compounds.[13,26,27] Indium is predominantly a by-product associated with inorganic substances such as clay minerals in zinc ores, and only a minor portion is linked to organic components. In addition, indium exhibits an affinity for copper. The occurrence state of critical metal elements refers to their chemical associations with other substances.[28] Revealing the occurrence state of critical metals within coal facilitates predictions regarding their migration and enrichment during coal processing and utilization.

In recent years, the transformation of strategic metal elements during the coal gasification process has also garnered widespread attention.[29–32] Coal gasification experiments and thermodynamic equilibrium calculations are frequently employed to predict and simulate the migration, transformation, and enrichment patterns of trace elements. It has been predicted that elements such as Ga, In, Hg, As, and Se are classified as volatile elements, which are likely to be present in the gas phase during gasification. Elements including Li, Zn, Mo, and Tb are identified as semi-volatile, while Re, Be, Ba, and V are categorized as non-volatile elements.[29,31,33] Due to the multi-source nature of minerals in coal, it remains challenging to study the source and formation mechanism of critical metals in coal. The occurrence state of most critical metals in coal is very complex, significantly influencing their thermal conversion behavior during coal gasification, including migration and enrichment. These elements can be released during coal gasification, causing adverse effects on both the ecological environment and human health.[33,34] Moreover, critical metals like lithium, gallium, germanium, and indium have significant industrial applications. Therefore, recovering and purifying these metals during coal gasification is of great significance. Thus, clarifying the critical metals' migration and enrichment state during coal gasification can provide crucial information for designing metal extraction schemes from gasification slag. In this work, a Late Carboniferous coal seam in the Jincheng area of Shanxi Province, China, with high concentrations of critical metal elements, was used as feed coal for gasification to investigate the migration and enrichment patterns under different reaction temperature conditions through element distribution analysis and molecular structure characterization.

2. Experimental

2.1 Materials

The primary raw material used in this study is the Late Carboniferous coal sourced from the Pingshuo region of Shanxi Province, China. The block coal underwent a series of processes to transform it into a finely powdered sample, including crushing, grinding, and sieving. Approximately 10 g of the Late Carboniferous coal was precisely measured and transferred to an alumina crucible for subsequent gasification experiments. The gasification process was carried out within a tube furnace under a controlled oxidizing atmosphere. The temperature of the furnace was gradually increased from ambient temperature to 1000 °C, 1100 °C, 1200 °C, 1300 °C, 1400 °C, and 1500 °C. A constant oxygen gas flow rate of 100 mL min⁻¹ is maintained throughout each heating cycle. A heating rate of 5 °C min⁻¹ was applied, with each soaking period lasting approximately 30 minutes at each target temperature point during the gasification experimentation. Consequently, distinct gasification slag prepared at different temperatures was labeled SX-10, SX-11, SX-12, SX-13, SX-14, and SX-15 for further analysis.

2.2 Characterizations

To determine the composition of the raw coal, both proximate and ultimate analyses were carried out. The proximate analysis followed the procedures outlined in the Chinese national standard (GB/T 212-2008). The ultimate analysis for the carbon and sulfur content was conducted using the LECO CS844 instrument (USA), whereas the LECO ONH836 instrument (USA) was employed to analyze the oxygen, nitrogen, and hydrogen content. X-ray fluorescence (XRF, Panalytical Axios, Netherlands) spectroscopy was used to identify the elemental composition of various samples. X-ray diffraction (XRD, Bruker D8 Advance, Rigaku, Japan) was used to analyze the crystal structure and composition of raw coal and gasification slags. This instrument operated with a Cu-Kα radiation source at an accelerating voltage of 40 kV and a current of 40 mA, scanning within the 2θ range from 5° to 70° with a step size of 0.02°. Fourier transform infrared (FTIR) spectroscopy (Spectrum GX, PerkinElmer, USA) was utilized to characterize the functional groups present in coal and its pyrolysis products. Scanning electron microscopy coupled with energy-dispersive X-ray spectroscopy (SEM-EDS, Gemini 300, Zeiss, Germany) provided insights into the morphological features and chemical compositions of the pyrolyzed samples. Raman spectroscopy (Raman, XPloRA Plus, Renishaw, UK) offered detailed information on the chemical structure of each sample. Finally, inductively coupled plasma-mass spectrometry (ICP-MS, NexION300D, PerkinElmer, USA) was employed to determine the distribution models and enrichment levels of the critical metal elements in different states.

2.3 Sequential chemical extraction

The distribution and enrichment levels of critical metal elements (Li, Ga, Ge, and In) in coal and gasification slags were investigated using a six-step sequential chemical extraction technique.
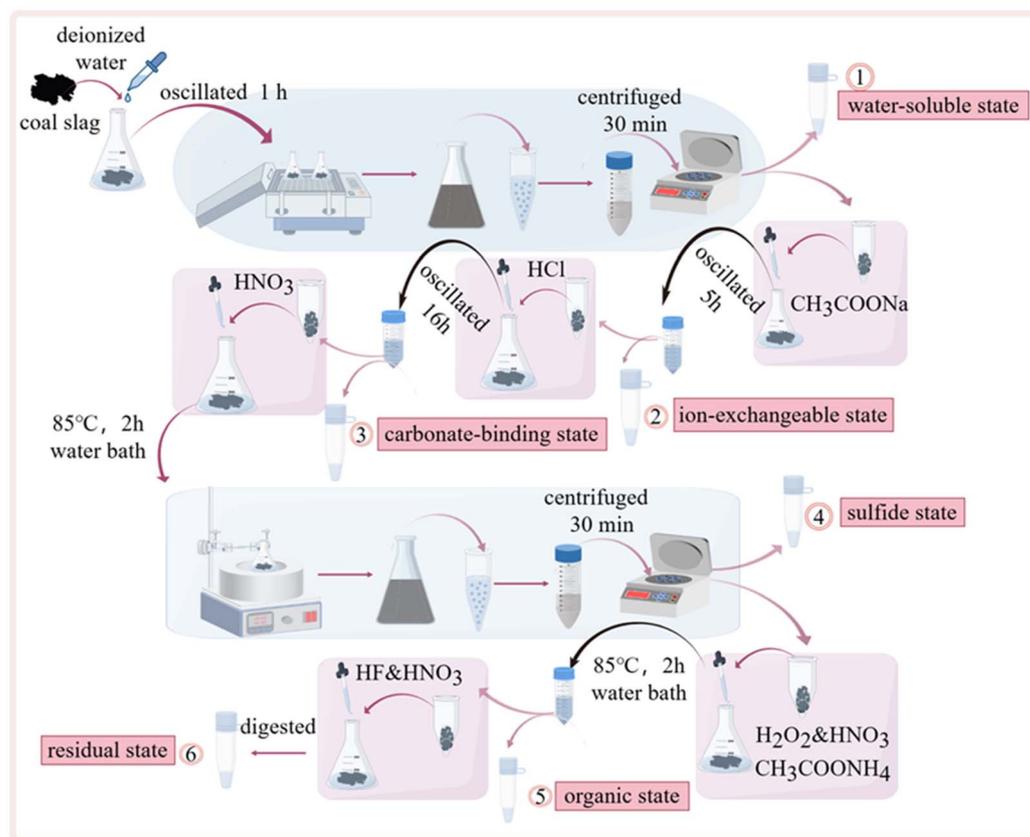
Fig. 1 Experimental process for sequential chemical extraction.

This approach categorized the elements into distinct fractions, including water-soluble, ion-exchangeable, carbonate-binding, sulfide, organic, and residual states.[35–39] The experimental procedure is shown in Fig. 1. About 1 g of coal and slag samples were accurately weighed, ground to a fine powder that passed through a 200-mesh sieve, and subsequently subjected to the six-step sequential chemical extraction method.[40]

2.4 Enrichment factor

To assess the migration of critical metal elements during coal gasification, the concentrations in coal and gasification slags were normalized with aluminum, silicon, and sulfur contents. The enrichment factor (EF) is then calculated using the formula below (eqn (1)).[41,42]

$$\text{EF} = \left[\frac{X_{\text{residue}}}{W_{\text{residue}}}\right] \bigg/ \left[\frac{X_{\text{coal}}}{W_{\text{coal}}}\right] \qquad (1)$$

where X_{residue} is the ratio of each critical element in different coal slags, μg g^{-1}; W_{residue} is the fraction of aluminum, silicon, and sulfur in slags, %; X_{coal} is the ratio of each critical metal in the coal, μg g^{-1}; and W_{coal} is the fraction of aluminum, silicon, and sulfur in raw coal, %.

2.5 Simulation

The thermodynamic equilibrium calculations of the critical metal elements were conducted utilizing FactSage 7.3, employing the principle of minimizing the Gibbs free energy.[43,44] FactSage 7.3 with FToxide and FactPs databases was utilized to predict the evolution of coal minerals during gasification. The system for calculation was meticulously defined based on the XRF analysis and ICP-MS results of the coal slag. The data required for these calculations encompassed carbon, hydrogen, oxygen, nitrogen, sulfur, silicon, aluminum, lithium, gallium, germanium, and indium. Thermodynamic equilibrium calculations were performed over a temperature range of 200 to 1500 °C, with intervals of 20 °C, under a high-pressure condition of 40 bar, replicating industrial gasification conditions.

3. Results and discussion

3.1 Composition and structure

The content of different oxide compositions is illustrated in Fig. 2(a) for both the coal sample and gasification slags. In raw coal, the Al_2O_3 content is less than 35%. As the gasification temperature increases, the Al_2O_3 concentration gradually rises, surpassing 40% at temperatures higher than 1100 °C. Compared to raw coal, the SiO_2 content in gasification slag is consistently higher than 40%. With increasing gasification temperature, the SO_3 content decreases from 6% to 2.5%. The CaO and Fe_2O_3 contents remain relatively stable with temperature changes, each accounting for approximately 5%.
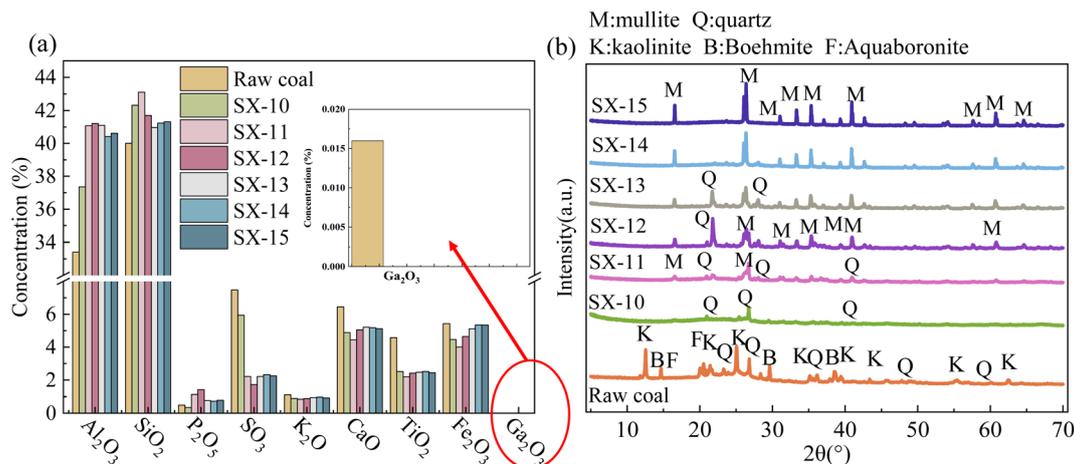
Fig. 2 XRF (a) with the inset showing a magnified view of the area marked by the red circle, and XRD (b) spectra of coal and different slags.

In comparison with raw coal, the TiO_2 content in gasification slag is reduced to about 2%. Notably, 0.01% Ga_2O_3 was detected in the raw coal, but no gallium oxide was found in the gasification slag, suggesting that gallium-containing compounds decompose at elevated temperatures. The mineral composition of the coal sample primarily consists of kaolinite, quartz, and boehmite, as shown in Fig. 2(b). At a gasification temperature of 1000 °C, kaolinite and boehmite decompose, leaving only quartz in the gasification slag. When the temperature exceeds 1100 °C, quartz begins to decompose and mullite forms. By 1400 °C, quartz has completely decomposed, and only mullite remains in the gasification slag, with a significant increase in the number and intensity of its signal peaks.

The FTIR spectra of the coal sample and gasification slags obtained at different temperatures are presented in Fig. 3(a).

The absorption peak of raw coal located at ~3500 cm⁻¹ corresponds to the –OH functional group, which cannot be observed in the spectra of gasification slags.[45] This suggests that hydroxyl-containing compounds are nearly absent in the gasification slag. The infrared signals at approximately 2800 cm⁻¹ and 2900 cm⁻¹ in raw coal are attributed to C–H stretching vibrations.[46] However, these peaks are only slightly discernible in the gasification slag, meaning there is a minimal presence of the aliphatic components. The absorption peak at around 1630 cm⁻¹ corresponds to the C=O stretching vibration in aromatic groups, while the peak at 1385 cm⁻¹ is associated with the stretching vibration of aromatic methyl groups. The Si–O vibration peak at 456 cm⁻¹ and the asymmetric stretching vibration of Si–O–Si at 802 cm⁻¹ demonstrate the formation of a silica framework in the gasification slag.[47–49] The Raman
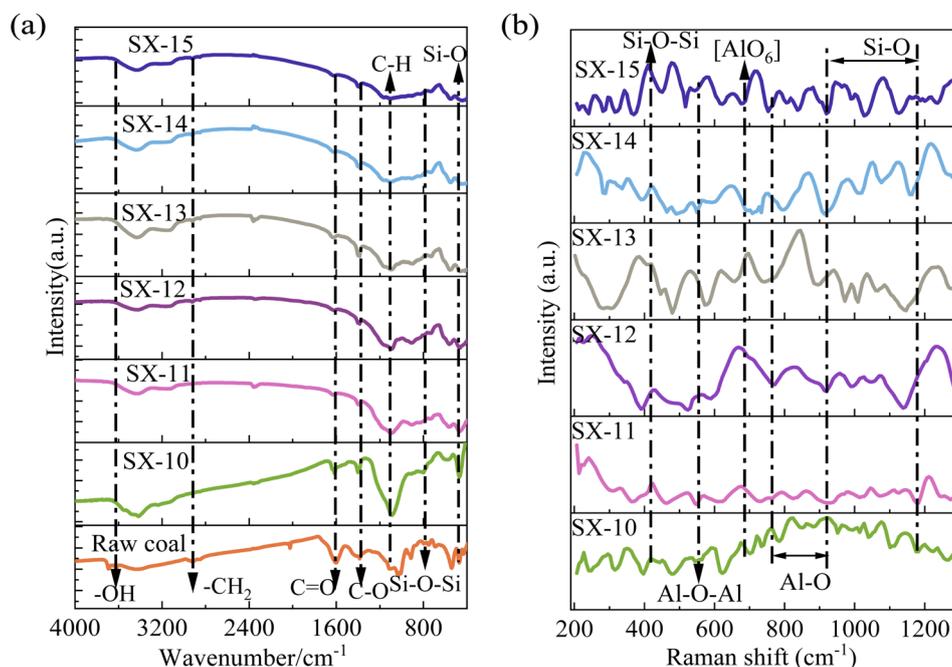

Fig. 3 FTIR (a) and Raman (b) spectra of coal and different slags.

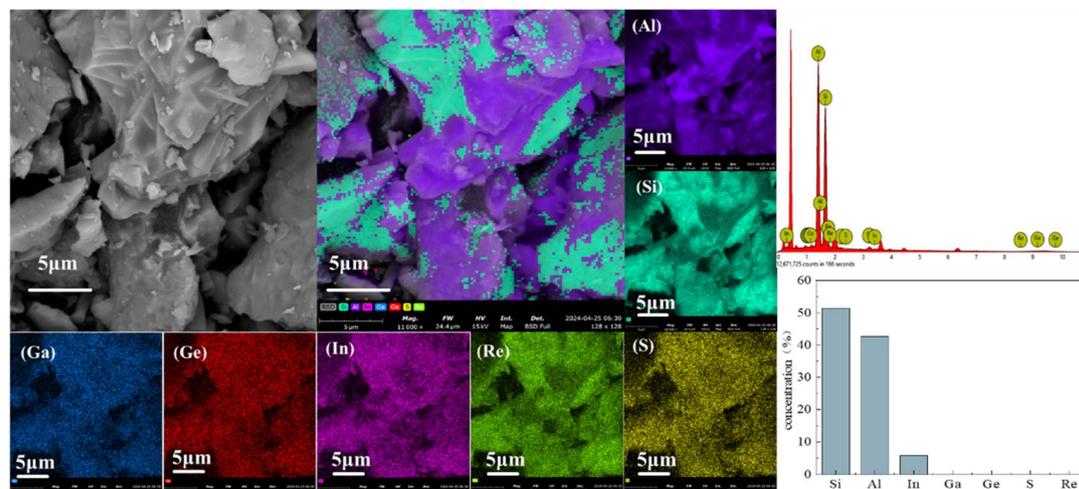© 2025 The Author(s). Published by the Royal Society of Chemistry

Fig. 4 SEM-EDS analysis of gasification slag obtained at 1500 °C.

spectra of the gasification slags are shown in Fig. 3(b). When the gasification temperature exceeds 1000 °C, the absence of characteristic D and G peaks in the Raman spectra reveals that the carbon in the coal has fully reacted with the oxidizing agent, thereby depleting the carbon content. Raman results show that the Si–O–Si bending vibration peak appears near 440 cm^{-1}, while the peak near 545 cm^{-1} corresponds to Al–O–Al bending vibrations.[50] The peak near 670 cm^{-1} is attributed to the Al–O stretching vibrations within the hexagonal aluminum oxide structures, and the peaks between 760 and 840 cm^{-1} are associated with the Al–O vibrations. The 860 to 1200 cm^{-1} region corresponds to the asymmetric stretching vibrations of the Si–O bonds.[51,52] These observations suggest that the gasification slag contains minimal residual carbon and organic matter, with its primary constituents being silica-aluminum minerals. These findings align with the infrared spectroscopy results.

SEM-EDS analysis was conducted on the gasification slag at 1500 °C, as illustrated in Fig. 4. The results indicate that Si and Al are predominant elements in the gasification slag, which aligns with the findings from the XRF and XRD analyses. Notably, 5.86% of the indium element was detected, and these elements were relatively uniformly distributed throughout the gasification slag. The surface concentrations of S, Ga, Ge, and Re in the gasification slag were extremely low, and these elements were not detected by SEM-EDS analysis.

3.2 Occurrence and enrichment

The distribution and enrichment concentrations of critical metal elements in different forms within raw coal and gasification slags are illustrated in Fig. 5. In raw coal, lithium is predominantly present in the residual fraction, with a concentration of around 1.2 $\mu g\ g^{-1}$, as depicted in Fig. 5(a). The concentrations of lithium in water-soluble, ion-exchangeable, carbonate-binding, sulfide, and organically bound forms are all less than 0.1 $\mu g\ g^{-1}$. Previous studies have indicated that lithium in coal is mainly associated with clay minerals, especially chlorite.[21,53] In the gasification slag obtained at different

temperatures, a large ratio of lithium elements remains in the residual form. In contrast, the lithium concentrations in water-soluble, ion-exchangeable, carbonate-binding, sulfide, and organically bound forms are all below 0.1 $\mu g\ g^{-1}$. As the gasification temperature rises, the residual lithium content shows a notable increase, rising from 1.2 $\mu g\ g^{-1}$ to 121.2 $\mu g\ g^{-1}$. It suggests that lithium is mainly associated with clay minerals in coal slag, and increasingly combines with silica-aluminate minerals at higher gasification temperatures. The changes in the occurrence form and enrichment content of gallium during gasification are illustrated in Fig. 5(b). The initial concentration of gallium in the residual form of raw coal is approximately 0.34 $\mu g\ g^{-1}$. In the gasification slag, gallium still predominantly exists in the residual form, and the enrichment content of the residual state gallium increases from 0.34 $\mu g\ g^{-1}$ to 46.93 $\mu g\ g^{-1}$ as the gasification temperature increases from 1000 °C to 1500 °C. The gallium concentration in the carbonate-binding state first rises and then falls with the increase of the gasification temperature, reaching a peak value of 0.87 $\mu g\ g^{-1}$ at 1200 °C. The concentrations of gallium in water-soluble, ion-exchangeable, sulfide, and organic forms in both the coal sample and gasification slags are all under 0.2 $\mu g\ g^{-1}$. As shown in Fig. 5(c), germanium mainly exists in a sulfide state in raw coal, followed by a carbonate-binding state and residual stat. Compared with raw coal, the germanium element in the gasification slag mainly remains in a residual state. It is worth mentioning that the contents of the carbonate-binding, sulfide, and residual states in the gasification slag increase significantly when the temperature is 1000 °C. The enrichment contents are 0.04 $\mu g\ g^{-1}$, 0.01 $\mu g\ g^{-1}$, and 0.23 $\mu g\ g^{-1}$, respectively. As the gasification temperature increases, the germanium content in the carbonate-binding and sulfide forms gradually decreases. Meanwhile, the germanium content in the residual fraction rises from 0.045 $\mu g\ g^{-1}$ to 0.12 $\mu g\ g^{-1}$ as the temperature increases from 1000 °C to 1500 °C. As shown in Fig. 5(d), indium in the coal sample is primarily enriched in the forms of carbonate-binding, sulfide, and residual states, with concentrations of $1 \times 10^{-3}\ \mu g\ g^{-1}$, $7 \times 10^{-3}\ \mu g\ g^{-1}$, and $6 \times 10^{-3}\ \mu g$
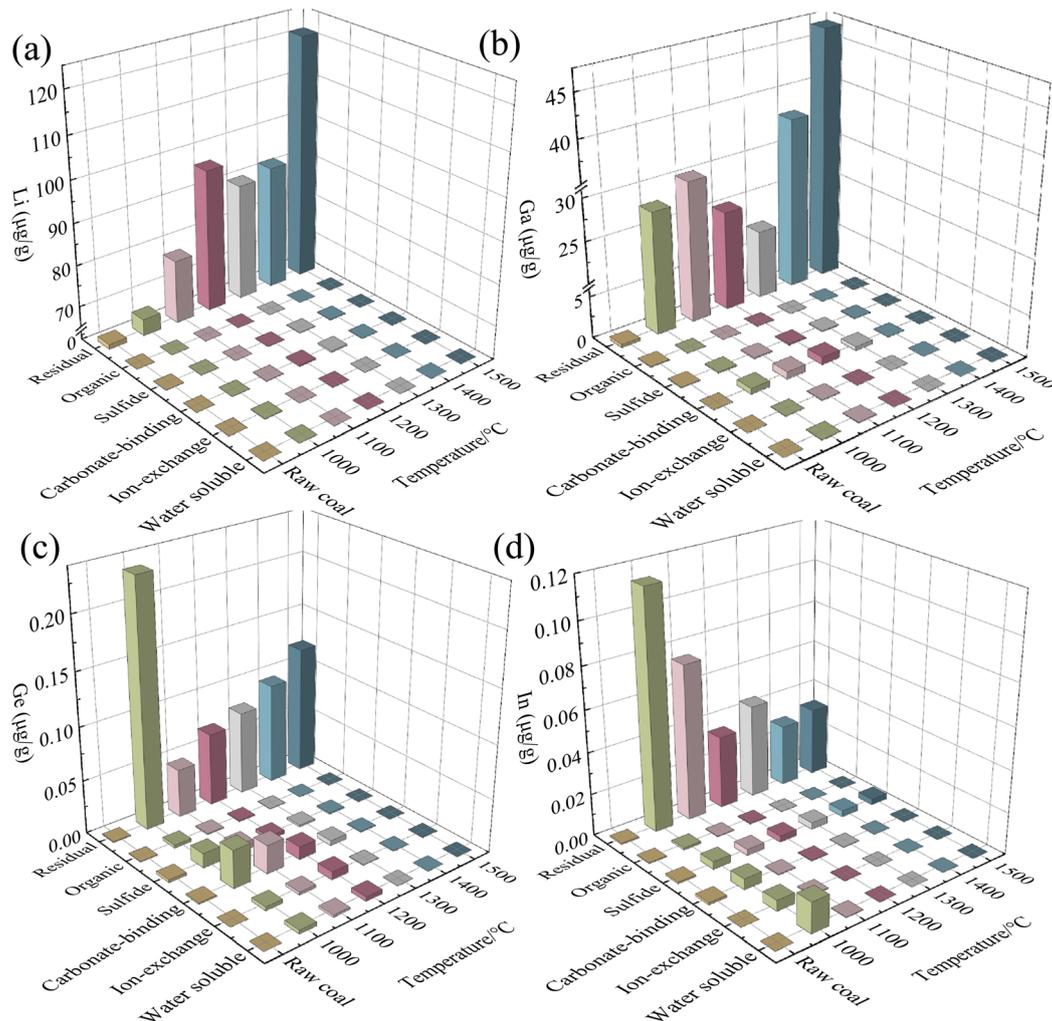
Fig. 5 Occurrence form and enrichment content of the critical metal elements: lithium (a), gallium (b), germanium (c), and indium (d).

g^{-1}, respectively. In raw coal, water-soluble and ion-exchangeable indium elements are almost absent. At a gasification temperature of 1000 °C, the concentrations of indium in water-soluble, ion-exchangeable, carbonate-binding, sulfide, and residual states significantly increase to 0.015 $\mu g\ g^{-1}$, 5 × $10^{-3}\ \mu g\ g^{-1}$, 5 × $10^{-3}\ \mu g\ g^{-1}$, 4 × $10^{-3}\ \mu g\ g^{-1}$, and 0.114 $\mu g\ g^{-1}$, respectively. After the gasification temperature reaches 1100 °C, the indium element predominantly remains in the residual state. As the gasification temperature increases, the residual indium content decreases from 0.114 $\mu g\ g^{-1}$ to 0.03 $\mu g\ g^{-1}$. Similarly, the concentrations of indium in water-soluble, ion-exchangeable, and carbonate-binding states also decrease with increasing gasification temperature. The indium concentration in the sulfide state remains relatively stable at approximately 4 × $10^{-3}\ \mu g\ g^{-1}$.

3.3 Enrichment relation and factor

Based on the concentrations of Al_2O_3, SiO_2, and SO_3 in raw coal and gasification slag, as determined by XRF analysis, the enrichment factors were calculated to evaluate the enrichment relationships between each critical metal element and the three oxides. The enrichment factor of different elements at different gasification temperatures is illustrated in Fig. 6. It is well known that the enrichment factors for lithium, gallium, germanium, and indium in coal gasification slags are all higher than 1, indicating that these elements are predominantly enriched in the slags. This result coincides well with the conclusion obtained by sequential chemical extraction measurement. As gasification temperature increases, the enrichment factors for lithium with both Al_2O_3 and SiO_2 exhibit an upward trend. It suggests that lithium is more likely to form compounds with Si and Al during gasification when the temperature is higher than 1400 °C, which aligns with the observed increase in the residual lithium content due to sequential chemical extraction. The enrichment factor for lithium and SO_3 increases to 1200 °C, while it decreases after 1200 °C, and then increases again at 1400 °C, revealing that the interaction between lithium and sulfide is unstable during gasification. The enrichment factors for gallium, Al_2O_3, SiO_2, and SO_3 show a similar V-shaped trend with temperature and reach the lowest values at 1300 °C, demonstrating a weak enrichment relationship between
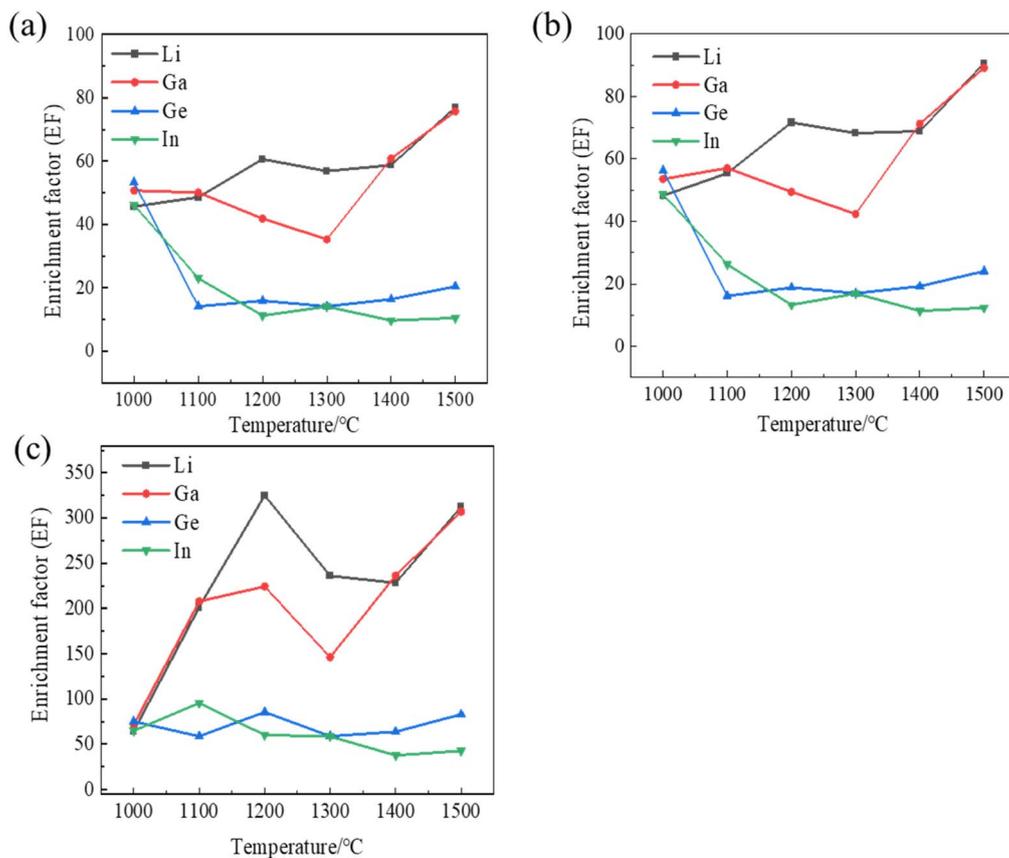
Fig. 6 Enrichment factor of different critical metal elements and Al_2O_3 (a), SiO_2 (b), and SO_3 (c).

gallium and these oxides in gasification. The enrichment factors for germanium and indium with Al_2O_3 and SiO_2 decrease significantly before 1100 °C, indicating weakened interactions, followed by a gradual stabilization after 1200 °C. The enrichment factors for germanium, indium, and SO_3 do not change significantly with temperature, indicating the relatively stable interactions with sulfur during gasification.

3.4 Simulation

The simulation results obtained using thermodynamic equilibrium methods are presented in Fig. 7. The transformation behavior of lithium is illustrated in Fig. 7(a). At gasification temperatures below 1200 °C, lithium predominantly exists as $LiAlSi_4O_{10}$ (s), indicating its association with silicates and aluminates. As the temperature exceeds 1200 °C, $LiAlSi_4O_{10}$ gradually decomposes into LiOH (g), completing this transformation by 1450 °C. Notably, the fraction of elemental lithium increases at 1400 °C, owing to its light and volatile properties. However, the molar fraction of elemental lithium remains at approximately 10% at 1500 °C, while the majority of lithium exists as LiOH (g) during high-temperature gasification. According to ICP-MS analysis, it was observed that as the gasification temperature increased from 1000 °C to 1500 °C, lithium predominantly existed in the residual state, with its content increasing from 1.2 μg g^{-1} to 121.2 μg g^{-1}. This demonstrates that lithium is mainly associated with clay minerals in coal slag.

Although $LiAlSi_4O_{10}$ is predicted to decompose when the temperature exceeds 1200 °C, it might be encased by the slag and is not completely volatile. The lithium is more inclined to combine with aluminates and silicates as the slag is cooled to atmospheric temperature. Fig. 7(b) shows the transformation behavior of gallium. Gallium primarily bonds with sulfur at lower gasification temperatures, forming Ga_2S_3 (s) and Ga_4S_5 (s). The decomposition of Ga_4S_5 is observed at 800 °C, producing Ga_2S (g), and it fully transforms into Ga_2S by 900 °C. As the temperature exceeds 1100 °C, the mole fraction of Ga_2S decreases, while the fractions of Ga_2O (g), GaH (g), and Ga (g) increase. Finally, the occurrence form and faction of gallium are Ga_2S, GaH, and Ga, which account for approximately 28%, 14%, and 58%, respectively. The mole fraction of different germanium-containing compounds is shown in Fig. 7(c). The germanium enriches mainly in the form of GeO_2 (s) at a relatively low temperature, and it converts to GeS (g) when the gasification temperature increases. Although a trace amount of GeO (g) is observed in the temperature range of 600 °C to 1500 °C, the predominant form of germanium during gasification is GeS. The transformation behavior of indium is presented in Fig. 7(d). At low temperatures, the indium appears as In_2S_3 (s), which comprises more than 80%. During the gasification reaction, In_2S_3 rapidly transforms into $In(OH)_2$. It should be ascribed to the strong oxidizing atmosphere during gasification. The mole fraction of $In(OH)_2$ decreases as the temperature
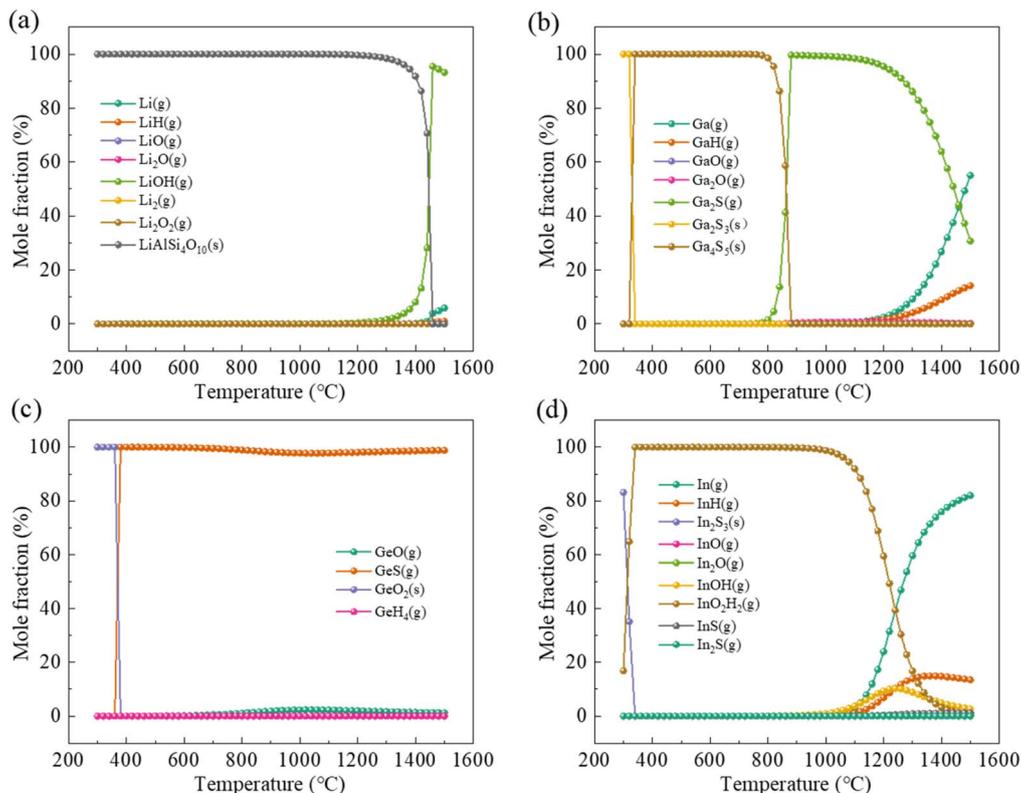
Fig. 7 Transformation behavior of lithium (a), gallium (b), germanium (c), and indium (d) assessed through FactSage simulation.

increases to 900 °C, and it converts into In (g), InH (g), InOH (g), and a small amount of InS (g). At 1500 °C, their molar ratios are approximately 83%, 13%, 3%, and 1%, respectively.

4. Conclusions

Elucidating the migration and enrichment dynamics of critical metals during coal gasification is beneficial to the development of metal extraction strategies from gasification slag. This study investigated the patterns of migration and enrichment under varying reaction temperatures through comprehensive element distribution analysis and molecular structure characterization, and the following conclusions were obtained. In the gasification slag obtained at temperatures above 1400 °C, quartz has completely decomposed, resulting in mullite—composed mainly of aluminates and silicates—as the main component. The signals corresponding to Si–O, O–Si–O, Al–O, and O–Al–O are observed in the FTIR and Raman spectra. As the gasification temperature increases from 1000 °C to 1500 °C, the lithium predominantly exists in the residual state, and its content improves from 1.2 μg g^{-1} to 121.2 μg g^{-1}. It demonstrates that lithium is mainly associated with clay minerals in coal slag. Although LiAlSi$_4$O$_{10}$ is predicted to decompose when the temperature exceeds 1200 °C, it might be encased by the slag and is not completely volatile. The lithium is more inclined to combine with aluminates and silicates as the slag is cooled to atmospheric temperature. Gallium is predominantly enriched in the residual form in the gasification slag, and the content of

residual state gallium increases from 0.34 μg g^{-1} to 46.93 μg g^{-1} as the gasification temperature increases from 1000 °C to 1500 °C. However, gallium is demonstrated to have a low affinity with aluminates and silicates in coal gasification slag, which is proven by enrichment factor analysis and thermodynamic simulation. Germanium in gasification slag mainly remains in a residual state when the gasification temperature reaches 1400 °C. According to the simulation results, germanium has more potential to combine with sulfur than aluminates and silicates, which coincides with the enrichment factor analysis. As the gasification temperature rises, the residual indium content drops from 0.114 μg g^{-1} to 0.03 μg g^{-1}. Meanwhile, the sulfide indium concentration is maintained at around 4×10^{-3} μg g^{-1}. As shown by the enrichment factor and thermodynamic simulation results, indium displays a complicated occurrence form in the coal slag, which presents a weak bonding ability with aluminates and silicates.

Data availability

The data used to support the findings of this study are available from the corresponding author upon request.

Author contributions

Juan Cai: writing – original draft, investigation, formal analysis, and data curation. Boyan Zhang: writing – review & editing, writing – original draft, validation, and investigation. Jiatao

Dang: writing – review & editing and validation. Yunpeng Zhao: writing – review & editing. Dingcheng Liang: writing – review & editing. Qiang Xie: writing – review & editing. Maohong Fan: writing – review & editing. Jinchang Liu: writing – review & editing, writing – original draft, validation, supervision, resources, project administration, methodology, investigation, funding acquisition, formal analysis, and conceptualization.

Conflicts of interest

The authors declare that they have no known competing financial interests or personal relationships that could have appeared to influence the work reported in this paper.

Acknowledgements

References

1 T. Popa, M. H. Fan, M. D. Argyle, R. B. Slimane, D. A. Bell and B. F. Towler, Catalytic gasification of a Powder River Basin coal, *Fuel*, 2013, **103**, 161–170, DOI: **10.1016/j.fuel.2012.08.049**.

2 F. Zhang, D. P. Xu, Y. G. Wang, M. D. Argyle and M. H. Fan, CO_2 gasification of Powder River Basin coal catalyzed by a cost-effective and environmentally friendly iron catalyst, *Appl. Energy*, 2015, **145**, 295–305, DOI: **10.1016/j.apenergy.2015.01.098**.

3 D. Yang, S. Li and S. He, Zero/negative carbon emission coal and biomass staged co-gasification power generation system via biomass heating, *Appl. Energy*, 2024, **357**, 122469, DOI: **10.1016/j.apenergy.2023.122469**.

4 X. Chen, L. Kong, J. Bai, X. Dai, H. Li, Z. Bai, *et al.*, The key for sodium-rich coal utilization in entrained flow gasifier: The role of sodium on slag viscosity-temperature behavior at high temperatures, *Appl. Energy*, 2017, **206**, 1241–1249, DOI: **10.1016/j.apenergy.2017.10.020**.

5 B. Lv, X. W. Deng, F. S. Jiao, B. B. Dong, C. J. Fang and B. L. Xing, Enrichment and utilization of residual carbon from coal gasification slag: A review, *Process Saf. Environ. Prot.*, 2023, **171**, 859–873, DOI: **10.1016/j.psep.2023.01.079**.

6 C. Wei, Y. T. Li, X. M. Liu, Z. Q. Zhang, P. F. Wu and J. R. Gu, Large-scale application of coal gasification slag in nonburnt bricks: Hydration characteristics and mechanism analysis, *Constr. Build. Mater.*, 2024, **421**, 135674–135683, DOI: **10.1016/j.conbuildmat.2024.135674**.

7 W. Wang, D. Liu, Y. Tu, L. Jin and H. Wang, Enrichment of residual carbon in entrained-flow gasification coal fine slag by ultrasonic flotation, *Fuel*, 2020, **278**, 118195, DOI: **10.1016/j.fuel.2020.118195**.

8 Y. Lu, Z. Li, Y. Wang, G. Jiang, F. Neng, C. Huang, *et al.*, Process design and thermal-calculation of a novel entrained-flow gasifier using fine ash as feedstock, *Appl. Energy*, 2023, **347**, 121395, DOI: **10.1016/j.apenergy.2023.121395**.

9 B. Lv, X. Deng, F. Jiao, B. Dong, C. Fang and B. Xing, Enrichment and utilization of residual carbon from coal gasification slag:A review, *Process Saf. Environ. Prot.*, 2023, **171**, 859–873, DOI: **10.1016/j.psep.2023.01.079**.

10 L. Ren, L. Ding, Q. Guo, Y. Gong, G. Yu and F. Wang, Characterization, carbon-ash separation and resource utilization of coal gasification fine slag: A comprehensive review, *J. Clean. Prod.*, 2023, **398**, 136554, DOI: **10.1016/j.jclepro.2023.136554**.

11 D. Liu, W. Wang, Y. Tu, G. Ren, S. Yan, H. Liu, *et al.*, Flotation specificity of coal gasification fine slag based on release analysis, *J. Clean. Prod.*, 2022, **363**, 132426, DOI: **10.1016/j.jclepro.2022.132426**.

12 C. Liao, Q. Li, W. Xuan, J. Zhang and J. Zhang, Comparative experimental study of ash formation behaviors during the fixed-bed gasification of coal water slurry and dry pulverized coal prepared from Shenmu coal, *Fuel*, 2024, **377**, 132762, DOI: **10.1016/j.fuel.2024.132762**.

13 S. F. Dai, R. B. Finkelman, D. French, J. C. Hower, I. T. Graham and F. H. Zhao, Modes of occurrence of elements in coal: A critical evaluation, *Earth-Sci. Rev.*, 2021, **222**, 103815–103890, DOI: **10.1016/j.earscirev.2021.103815**.

14 Q. F. Lu, S. J. Qin, W. F. Wang, Q. Wang and S. Kang, Geochemistry of Late Permian coals from the Yueliangtian coal deposit, Guizhou: Evidence of sediment source and evaluation on critical elements, *Sci. Total Environ.*, 2023, **856**, 159123–159136, DOI: **10.1016/j.scitotenv.2022.159123**.

15 Q. Z. Qin, J. S. Deng, H. H. Geng, Z. Y. Bai, X. H. Gui, Z. T. Ma, *et al.*, An exploratory study on strategic metal recovery of coal gangue and sustainable utilization potential of recovery residue, *J. Clean. Prod.*, 2022, **340**, 130765–130776, DOI: **10.1016/j.jclepro.2022.130765**.

16 F. R. Field, T. J. Wallington, M. Everson and R. E. Kirchain, Strategic Materials in the Automobile: A Comprehensive Assessment of Strategic and Minor Metals Use in Passenger Cars and Light Trucks, *Environ. Sci. Technol.*, 2017, **51**(24), 14436–14444, DOI: **10.1021/acs.est.6b06063**.

17 E. O. Opare, E. Struhs and A. Mirkouei, A comparative state-of-technology review and future directions for rare earth element separation, *Renew. Sustain. Energy Rev.*, 2021, **143**, 110917, DOI: **10.1016/j.rser.2021.110917**.

18 C. H. Choi, J. Eun, J. J. Cao, S. Lee and F. Zhao, Global strategic level supply planning of materials critical to clean energy technologies - A case study on indium, *Energy*, 2018, **147**, 950–964, DOI: **10.1016/j.energy.2018.01.063**.

19 G. Harper, R. Sommerville, E. Kendrick, L. Driscoll, P. Slater, R. Stolkin, *et al.*, Recycling lithium-ion batteries from electric vehicles, *Nature*, 2019, **575**(7781), 75–86, DOI: **10.1038/s41586-019-1682-5**.

20 E. A. Olivetti, G. Ceder, G. G. Gaustad and X. K. Fu, Lithium-Ion Battery Supply Chain Considerations: Analysis of Potential Bottlenecks in Critical Metals, *Joule*, 2017, **1**(2), 229–243, DOI: 10.1016/j.joule.2017.08.019.

21 S. Dai, R. B. Finkelman, D. French, J. C. Hower, I. T. Graham and F. Zhao, Modes of occurrence of elements in coal: A critical evaluation, *Earth-Sci. Rev.*, 2021, **222**, 103815, DOI: 10.1016/j.earscirev.2021.103815.

22 V. Balaram, M. Santosh, M. Satyanarayanan, N. Srinivas and H. Gupta, Lithium: A review of applications, occurrence, exploration, extraction, recycling, analysis, and environmental impact, *Geosci. Front.*, 2024, **15**(5), 5–50, DOI: 10.1016/j.gsf.2024.101868.

23 A. Valero, A. Valero, G. Calvo and A. Ortego, Material bottlenecks in the future development of green technologies, *Renew. Sustain. Energy Rev.*, 2018, **93**, 178–200, DOI: 10.1016/j.rser.2018.05.041.

24 M. X. Zhou, S. F. Dai, X. B. Wang, L. Zhao, V. P. Nechaev, D. French, *et al.*, Critical element (Nb-Ta-Zr-Hf-REE-Ga-Th-U) mineralization in Late Triassic coals from the Gaosheng Mine, Sichuan Basin, southwestern China: Coupled effects of products of sediment-source-region erosion and acidic water infiltration, *Int. J. Coal Geol.*, 2022, **262**, 104101–104119, DOI: 10.1016/j.coal.2022.104101.

25 Z. Zhao, L. Cui, Y. Guo, H. Li and F. Cheng, Recovery of gallium from sulfuric acid leach liquor of coal fly ash by stepwise separation using P507 and Cyanex 272, *Chem. Eng. J.*, 2020, **381**, 122699, DOI: 10.1016/j.cej.2019.122699.

26 J. Liu, B. F. Spiro, S. Dai, D. French, I. T. Graham, X. Wang, *et al.*, Strontium isotopes in high- and low-Ge coals from the Shengli Coalfield, Inner Mongolia, northern China: New indicators for Ge source, *Int. J. Coal Geol.*, 2021, **233**, 103642–103652, DOI: 10.1016/j.coal.2020.103642.

27 Q. Wei, S. B. Wang, L. Zhao and J. H. Zou, Modes of occurrence of organically-associated arsenic in Ge-rich coal deposits, *Fuel*, 2024, **371**, 132067–132077, DOI: 10.1016/j.fuel.2024.132067.

28 J. Ribeiro, G. Machado, N. Moreira, I. Suárez-Ruiz and D. Flores, Petrographic and geochemical characterization of coal from Santa Susana Basin, Portugal, *Int. J. Coal Geol.*, 2019, **203**, 36–51, DOI: 10.1016/j.coal.2019.01.005.

29 J. R. Bunt and F. B. Waanders, Trace element behaviour in the Sasol-Lurgi fixed-bed dry-bottom gasifier. Part 3-The non-volatile elements: Ba, Co, Cr, Mn, and V, *Fuel*, 2010, **89**(3), 537–548, DOI: 10.1016/j.fuel.2009.04.018.

30 J. Chen, J. J. Wu, Y. X. Zhang, Y. Guo, L. Yan and J. Li, Transformation of typical heavy metals during preparation of porous carbon from coal gasification fine slag, *J. Environ. Chem. Eng.*, 2024, **12**(5), 113734–113750, DOI: 10.1016/j.jece.2024.113734.

31 R. Yoshiie, Y. Taya, T. Ichiyanagi, Y. Ueki and I. Naruse, Emissions of particles and trace elements from coal gasification, *Fuel*, 2013, **108**, 67–72, DOI: 10.1016/j.fuel.2011.06.011.

32 S. Q. Liu, C. Qi, Z. Jiang, Y. J. Zhang, M. F. Niu, Y. Y. Li, *et al.*, Mineralogy and geochemistry of ash and slag from coal gasification in China: a review, *Int. Geol. Rev.*, 2018, **60**(5–6), 717–735, DOI: 10.1080/00206814.2017.1287013.

33 Y. Wang, Y. Tang, S. Liu, Y. Wang, R. B. Finkelman, B. Wang, *et al.*, Behavior of trace elements and mineral transformations in the super-high organic sulfur Ganhe coal during gasification, *Fuel Process. Technol.*, 2018, **177**, 140–151, DOI: 10.1016/j.fuproc.2018.04.019.

34 Y. F. Wang, Y. G. Tang, X. Guo, Q. Xie, R. B. Finkelman, P. Y. Li, *et al.*, Fate of potentially hazardous trace elements during the entrained-flow coal gasification processes in China, *Sci. Total Environ.*, 2019, **668**, 854–866, DOI: 10.1016/j.scitotenv.2019.03.076.

35 J. A. Galhardi, B. P. Leles, J. W. V. de Mello and K. J. Wilkinson, Bioavailability of trace metals and rare earth elements (REE) from the tropical soils of a coal mining area, *Sci. Total Environ.*, 2020, **717**, 134484–134497, DOI: 10.1016/j.scitotenv.2019.134484.

36 W. P. Ma, Z. Li, J. F. Lv, L. H. Yang and S. Q. Liu, Environmental evaluation study of toxic elements (F, Zn, Be, Ni, Ba, U) in the underground coal gasification (UCG) residuals, *J. Clean. Prod.*, 2021, **297**, 126565–126578, DOI: 10.1016/j.jclepro.2021.126565.

37 W. Feng, Z. J. Wan, J. Daniels, Z. K. Li, G. K. Xiao, J. L. Yu, *et al.*, Synthesis of high quality zeolites from coal fly ash: Mobility of hazardous elements and environmental applications, *J. Clean. Prod.*, 2018, **202**, 390–400, DOI: 10.1016/j.jclepro.2018.08.140.

38 L. Tong, J. He, F. Wang, Y. Wang, L. Wang, D. C. W. Tsang, *et al.*, Evaluation of the BCR sequential extraction scheme for trace metal fractionation of alkaline municipal solid waste incineration fly ash, *Chemosphere*, 2020, **249**, 126115, DOI: 10.1016/j.chemosphere.2020.126115.

39 F. Xu, S. J. Qin, S. Y. Li, J. X. Wang, D. E. Qi, Q. F. Lu, *et al.*, Distribution, occurrence mode, and extraction potential of critical elements in coal ashes of the Chongqing Power Plant, *J. Clean. Prod.*, 2022, **342**, 130910–130921, DOI: 10.1016/j.jclepro.2022.130910.

40 J. Cai, B. Zhang, J. Dang, Y. Zhao, D. Liang, Q. Xie, *et al.*, Migration, transformation, and enrichment of strategic metal elements including Li, Ga, Ge, In, and Re during the coal pyrolysis process, *J. Anal. Appl. Pyrolysis*, 2025, **186**, 106953, DOI: 10.1016/j.jaap.2025.106953.

41 Y. F. Wang, Y. G. Tang, S. Q. Liu, Y. G. Wang, R. B. Finkelman, B. L. Wang, *et al.*, Behavior of trace elements and mineral transformations in the super-high organic sulfur Ganhe coal during gasification, *Fuel Process. Technol.*, 2018, **177**, 140–151, DOI: 10.1016/j.fuproc.2018.04.019.

42 X. Guo, Y. G. Tang, Y. F. Wang, C. F. Eble, R. B. Finkelman, B. B. Huan, *et al.*, Potential utilization of coal gasification residues from entrained-flow gasification plants based on rare earth geochemical characteristics, *J. Clean. Prod.*, 2021, **280**, 124329–124343, DOI: 10.1016/j.jclepro.2020.124329.

43 D. Liang, Q. Xie, Z. Wei, C. Wan, G. Li and J. Cao, Transformation of alkali and alkaline earth metals in Zhundong coal during pyrolysis in an entrained flow bed

reactor, *J. Anal. Appl. Pyrolysis*, 2019, **142**, 104661–104671, DOI: **10.1016/j.jaap.2019.104661**.

44 X. S. Wang, T. D. Ma, Y. G. Tang, R. Gupta, H. H. Schobert and J. Y. Zhang, Volatilization of Potentially Harmful Trace Elements in Coal Pyrite during Heat Treatment in a Tube Furnace at 573-1473 K, *Energy Fuels*, 2023, **37**(17), 12716–12727, DOI: **10.1021/acs.energyfuels.3c01253**.

45 B. Jiang, C.-F. Yu, L. Yuan, K. Lu, W. Tao, H. Lin, *et al.*, Investigation on oxidative pyrolysis characteristics of bituminous coal through thermal analysis and density functional theory, *Appl. Energy*, 2023, **349**, 121680, DOI: **10.1016/j.apenergy.2023.121680**.

46 F. Gao, Z. Jia, Z. Cui, Y.-d Li and H. Jiang, Evolution of macromolecular structure during coal oxidation via FTIR, XRD and Raman, *Fuel Process. Technol.*, 2024, **262**, 108114, DOI: **10.1016/j.fuproc.2024.108114**.

47 A. D. Kamble, V. A. Mendhe, P. D. Chavan and V. K. Saxena, Insights of mineral catalytic effects of high ash coal on carbon conversion in fluidized bed Co-gasification through FTIR, XRD, XRF and FE-SEM, *Renew. Energy*, 2022, **183**, 729–751, DOI: **10.1016/j.renene.2021.11.022**.

48 Y. Zhao, L. Liu, P. H. Qiu, X. Xie, X. Y. Chen, D. Lin, *et al.*, Impacts of chemical fractionation on Zhundong coal's chemical structure and pyrolysis reactivity, *Fuel Process. Technol.*, 2017, **155**, 144–152, DOI: **10.1016/j.fuproc.2016.05.011**.

49 Q. Z. Qin, H. H. Geng, J. S. Deng, X. B. Su, M. Chen and C. B. Park, Al and other critical metals co-extraction from coal gangue through delamination pretreatment and recycling strategies, *Chem. Eng. J.*, 2023, **477**, 147036–147045, DOI: **10.1016/j.cej.2023.147036**.

50 J. Qin, W. Liu, H. Wu, J. Wang, Q. Xue, H. Zhao, *et al.*, A comprehensive investigation on the viscosity and structure of CaO-SiO2-Al2O3-MgO-BaO slag with different Al2O3/SiO2 ratios, *J. Mol. Liq.*, 2022, **365**, 120060, DOI: **10.1016/j.molliq.2022.120060**.

51 W. Yan, G. Zhang and J. Li, Viscosity and structure evolution of CaO–SiO2-based mold fluxes with involvement of CaO–Al2O3-based tundish fluxes, *Ceram. Int.*, 2020, **46**(9), 14078–14089, DOI: **10.1016/j.ceramint.2020.02.208**.

52 W. Guo, J. Wu, X. Liu and J. Wang, Raman and X-ray photoelectron spectroscopy study on the influence of La2O3 on the melt structure of SiO2–CaO–Al2O3–MgO, *Ceram. Int.*, 2022, **48**(18), 25933–25939, DOI: **10.1016/j.ceramint.2022.05.270**.

53 F. Xu, S. J. Qin, S. Y. Li, H. J. Wen, D. W. Lv, Q. Wang, *et al.*, The migration and mineral host changes of lithium during coal combustion: Experimental and thermodynamic calculation study, *Int. J. Coal Geol.*, 2023, **275**, 104298–104311, DOI: **10.1016/j.coal.2023.104298**.